

(GAN), which achieved an 85.23% recognition rate with 20 samples for each target [9]. Gao et al. proposed a semi-supervised GAN with multiple generators, which achieved more than 92% with around 40 samples in each target type [10].

The metric-based methods are based on learning representations for classes that can generalize to new classes. For example, Li et al. proposed a conv-biLSTM prototypical network, which has a classifier based on the Euclidean distance between training samples and the prototypical of each class [11]. Fu et al. designed a hard task mining method for effective meta-learning which yields better performance with the largest absolute improvements of 1.7% and 2.3% for 1-shot and 5-shot, respectively [12]. The model-based methods use prior knowledge to construct the embedding space and constrain the complexity. For example, Persello et al. proposed an active and semi-supervised learning network for SAR ATR, which is a semi-supervised support vector machine (SVM) [13]. Li et al. proposed a classification approach that adopts the canonical scattering models widely used in model-based decompositions to provide an improvement for the well-known H/α classification [14].

However, the challenge of FSL in SAR ATR is whether to have a helpful inductive bias [15–17], which can improve performance on novel classes but is hard to develop when the feature embedding has a large difference between a few samples and full samples [15,18]. In essence, these methods above just further mine the few labeled SAR images to obtain more usable recognition information. During the process, these methods cannot acquire new information from these few samples in terms of information theory, which hinders the improvement of recognition performance in SAR images.

In the light of deep segmentation methods for SAR images [19,20], the target segmentation has become more achievable and can reveal the unique morphological features that can be extended for use to SAR ATR under a few labeled training SAR samples. For example, Ref. [21] proposed a differentiable superpixel generation method and a superpixelwise statistical dissimilarity measure method with the encoder–decoder structure. Ref. [22] proposed one differentiable boundary-aware clustering method and the soft association map with an encoder–decoder structure. Meanwhile, the segmentation of SAR images is also beneficial for the SAR civil application [23,24]. For example, the segmentation of SAR images can help terrain mapping in debris flow rescue or urban construction design. Therefore, the segmentation of SAR images can be a basic and functional research field in SAR application.

To address the FSL challenge of SAR ATR, our key objective is to exploit the transductive generalization on unlabeled samples with an auxiliary loss serving as a regularizer. In doing so, not only the induction bias can be improved by narrowing the difference between a few samples and full samples, but also the transductive generalization can be exploited through an auxiliary loss. In this paper, we propose a semi-supervised SAR ATR framework with auxiliary segmentation (SFAS). This framework utilizes the core idea of transductive generalization to explore the relative features between unlabeled SAR samples and a few labeled SAR samples. Through auxiliary segmentation of unlabeled SAR samples and information residue loss (IRL) in training, the effectiveness of features extracted by the network is boosted, and the recognition of few labeled SAR samples is promoted greatly. In addition, accurate segmentation is also beneficial for SAR image interpretation, such as precision location or topographic mapping. The framework consists of three blocks: a shared feature extractor, a classifier to accomplish the recognition of labeled SAR target images, and a decoder to accomplish the segmentation of the unlabeled SAR target images. The contributions are as follows:

1. We focus on the transductive generalization on unlabeled samples and proposed a semi-supervised SAR ATR algorithm with an auxiliary segmentation loss as a regularizer, which improves the inductive bias of the model and provides a new source of abundant feature information for high recognition performance of SAR ATR FSL.

2. To explore the relative features between unlabeled SAR samples and few labeled SAR samples, we construct a training loop process (TCL) to alternately perform a semi-blind training optimization, and an information residue loss (IRL) to build a progressive optimization of recognition and segmentation. It can help the model optimize towards information compilation of segmentation and recognition.
3. The proposed framework achieves competitive performance to state-of-the-art methods on standard benchmarks and is easy to follow. The recognition rates of 40 training samples in each class are above 95.50%, and the rates of 20 training samples in each class are above 94.00%.

The remainder of this paper is organized as follows: the framework of the proposed SFAS and detailed information about some modules are presented in Section 2. Section 3 demonstrates the evaluation of performance based on the experimental results. Finally, Section 4 draws a brief conclusion.

2. Proposed Method

The motivation of the proposed algorithm is to utilize unlabeled samples which are relative to a few labeled SAR samples to explore the transductive generalization from unlabeled to few labeled. Limited by the practical circumstances, SAR ATR has to face the recognition of FSL, which leads to most of the existing methods failing to learn a helpful inductive bias on a few labeled samples. Nevertheless, in reality, there are often abundant unlabeled SAR samples which have a similar distribution with few labeled samples. By exploring the transductive generalization of unlabeled samples on an effective algorithm, the recognition of FSL in SAR ATR can be promoted and achieve state-of-the-art performance.

In this section, the proposed SFAS is introduced. First, we elucidate the training loop process and framework of the SFAS. Then, the information residue loss and specific baseline of the network are described in detail. To avoid confusion, it is specifically stated here that, in our paper, the labeled samples refer to the data with class labels but without segmentation labels, while unlabeled samples refer to the data with segmentation labels but without class labels.

2.1. Training Loop and Framework of Proposed SFAS

To explore the transductive generalization of unlabeled samples, we focus on extracting more generalized and effective features. Thus, we proposed a training loop process to make the network learn from multiple tasks and seek more generalized features which satisfy the optimization of multi-task. The description of the novel training loop is as follows.

As shown in Figure 1, during the training, there are mainly two steps: training data generating and training loop. In the training data generating phase, the random generator generates the unlabeled and labeled set required in the training process by sampling randomly from the training set. In addition, in one training loop, there is twice semi-blind training for recognition and segmentation.

We use D_U to denote the unlabeled set, D_L to denote the labeled set, M_E , M_D , M_C to denote the extractor, decoder, and classifier, and P_E , P_D , and P_C to denote the corresponding learnable parameters. In the first semi-blind training in one training loop, the unlabeled set D_U goes through extractor M_E and decoder M_D to calculate a segmentation loss L_S . The segmentation loss L_S is only employed to update P_D , and L_S are combined with recognition loss L_R of the last training loop based on IRL to update P_E . Then, in the second semi-blind training, the few labeled set D_L goes through extractor M_E and decoder M_C to calculate a segmentation loss L_R . The loss L_R is only employed to update P_C , and L_R are combined with L_S based on IRL to update P_E again.

By alternately performing semi-blind training for recognition and segmentation, this training loop can gradually exploit the transductive information of unlabeled samples to construct a helpful inductive bias on a few labeled samples.

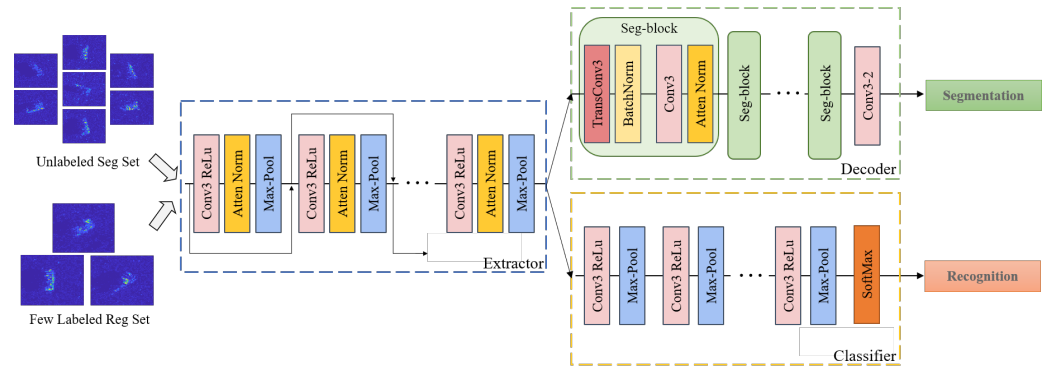


Figure 1. Baseline architecture.

Besides the shared feature extractor, a classifier and a decoder are shown in Figure 1, and the batch normalization and attention mechanism are employed in some level of multi-level feature extractors to ensure the network focus on the more effective features among the extracted features.

2.2. Information Residue Loss

The basic segmentation and recognition loss are set as the same form of cross-entropy cost. It should be noted that the design of the loss function for the classifier and decoder can promote each other and improve the accuracy simultaneously because the same form of loss can help construct the manifold structure and similar constraints. The details are as follows.

The recognition loss is set as the cross-entropy cost function, which is presented as

$$L_r(\mathbf{w}, \mathbf{b}) = - \sum_{i=1}^C y_i \log(p(y_i|\mathbf{x})), \tag{1}$$

where $p(y_i|\mathbf{x})$ is the probability vector of recognition result of the i th SAR chip, y_i is the recognition labels, and C is the number of the recognition classes.

The function of the segmentation loss is defined as

$$L_s(\mathbf{w}, \mathbf{b}) = - \frac{1}{n} \sum_{i=1}^V \mathbf{s}_i \log(m(\mathbf{s}_i|\mathbf{x})), L_s(\mathbf{w}, \mathbf{b}) = - \frac{1}{n} \sum_{i=1}^V s_i \log(m(s_i|\mathbf{x})), \tag{2}$$

where $\mathbf{m}(\mathbf{s}_i|\mathbf{x})$ is the binary matrix of segmentation result of all pixel on the i th SAR chip, n is the number of pixels in a SAR chip, \mathbf{s}_i is the segmentation labels, and V is the number of the segmentation types.

Then, during the proposed training loop, the recognition loss is constructed based on the proposed information residue loss by combining the segmentation loss of the last training loop. The calculation is as follows.

For the recognition loss of IRL, it is defined as:

$$L_r^t = - \sum_{i=1}^C y_i^t \log(p^t(y_i^t|x^{(L,t)})) - \frac{\alpha}{n} \sum_{i=1}^V \mathbf{s}_i^{t-1} \log(\mathbf{p}^{t-1}(\mathbf{s}_i^{t-1}|x^{(L,t-1)})), \tag{3}$$

where t is the training steps, and α denotes the parameter to adjust the residue ratio of segmentation information of the last loop.

The computation of the parameter α in IRL is

$$\alpha = \frac{-1}{t} + 1. \tag{4}$$

[3] We have corrected the expressions to be consistent.

For the segmentation loss of IRL, the function is

$$L_s^t = -\frac{1}{n} \sum_{i=1}^V s_i^t \log\left(\mathbf{p}^t\left(\mathbf{s}_i^t \mid x^{(L,t)}\right)\right) - \alpha \sum_{i=1}^C y_i^{t-1} \log\left(p^{t-1}\left(y_i^{t-1} \mid x^{(L,t-1)}\right)\right) \quad (5)$$

The proposed novel IRL utilizes the combination of the current recognition loss and information residue of previous segmentation loss to update the extractor or vice versa. This technology, at first, can lead to more effective optimization separately for recognition and segmentation. Then, when the training is going on, the integration of the losses of both recognition and segmentation can make the optimization of the extractor towards higher accuracy of the recognition and segmentation simultaneously, and further force the network gradually extract more generalized and effective features from unlabeled and labeled samples. It is helpful to exploit the transductive generalization from unlabeled samples to construct an effective inductive bias on a few labeled SAR samples.

Therefore, the proposed SFAS not only enables few-shot learning by employing unlabeled SAR target images but also provides an effective way to apply deep learning SAR ATR methods in practical applications by acquiring a small amount of labeled SAR images and various flexible SAR images as an auxiliary task.

2.3. Baseline Architecture

To exploit the transductive generalization on unlabeled samples with an auxiliary loss, each part of the architecture needs to be designed carefully. To extract more generalized and effective features for recognition and segmentation, the shared feature extractor needs to face the two challenges of recognition and segmentation in the training process. The classifier and decoder for the recognition and segmentation respectively need to employ the fine-tune of downstream subtasks.

Therefore, the baseline architecture is designed as shown in Figure 1. From the shared extractor in the blue box of Figure 1, the convolutional layers are linked by the residual way, and the attention mechanism block that contains spatial and channel attention modules [25] is employed to focus on the crucial local feature and compress the useless information in each layer. In addition, the leaky ReLu and batch normalization are employed to improve the generalization of the extractor.

The decoder shown in the green box of Figure 1 is mainly constructed by trans-convolutional blocks. These blocks consist of a trans-convolutional layer to reconstruct the structure of the SAR images, and a convolutional layer with attention and batch normalization to increase the generalization. Finally, a segmentation layer (Conv3-2) outputs the segmentation results. The classifier shown in the yellow box of Figure 1 is simply stacking the convolutional layer and max-pool layer to control the parameter of the classifier, which is an effective structure of classifier in SAR ATR.

Through the method described above, the recognition of SAR ATR under limited training data has the potential to achieve high performance. The next section shows the experiments and the results.

3. Experimental Results

In this section, the dataset for evaluation is presented. Then, we evaluated the performance of recognition and auxiliary segmentation under different sample numbers to validate the effectiveness and the transductive information of the proposed SFAS.

3.1. Dataset and Network Setup

The MSTAR dataset is a benchmark dataset for the SAR ATR performance assessment. The dataset contains a series of $0.3 \text{ m} \times 0.3 \text{ m}$ SAR images of ten different classes of ground targets. The optical images and corresponding SAR images of ten classes of targets in the MSTAR dataset are shown in Figure 2. The training and testing data have the same ten target classes but different depression angles. The training data are captured under

a depression angle of 17° , and the testing data are captured under that of 15° . It should be noted the ground truth of segmentation is roughly acquired by manual annotation using the tool named OpenLabeling, and there are also many available accurate automatic methods [19,20] to segment. The distribution of the training and testing images is listed in Table 1.

Table 1. MSTAR dataset used in experiments.

Target Type	BMP2	BRDM2	BTR60	BTR70	D7	2S1	T62	T72	ZIL131	ZSU235
Training (17°)	233	298	256	233	299	299	299	232	299	299
Testing (15°)	195	274	195	196	274	274	273	196	274	274

The hyperparameters in the proposed network are included in Table 2. The input SAR images have the size 80×80 . For each convolutional layer, the size of the stride is set as 1×1 . For each max-pooling layer, the size of the stride is set as 2×2 . The batch size is set as 64, and the learning rate is initialized as 0.0001. The labeled samples are based on the selected labeled training sample number in the experiments, and are randomly chosen from the whole dataset; then, the rest of the dataset is regarded as the unlabeled training samples. For example, if the number of selected labeled training samples is 60 for each class, it means that for each class, there are 60 randomly chosen labeled samples if the selected labeled training sample number is 60 for each class, 60 labeled samples for each class are randomly chosen from the whole dataset, and the rest of the samples for each class are set as the unlabeled samples. -

[4] We have rewritten the sentence.

[5] We replaced * with \times in Table 2 to make it clear.

Table 2. Hyper-parameters of the proposed framework.

Module	Layers	BatchNorm or Attention
Extractor	Conv $3 \times 3 @ 16$	BatchNorm
	ReLU + MaxPool	Neither
	Conv $3 \times 3 @ 32$	BatchNorm
	ReLU + MaxPool	Neither
	Conv $3 \times 3 @ 64$	Both
	ReLU + MaxPool	Neither
Decoder	Trans-Conv $3 \times 3 @ 64$	BatchNorm
	Conv $3 \times 3 @ 32$	Both
	Trans-Conv $3 \times 3 @ 32$	BatchNorm
	Conv $3 \times 3 @ 16$	Both
	Trans-Conv $3 \times 3 @ 16$	BatchNorm
	Conv $3 \times 3 @ 8$	Neither
Classifier	Conv $3 \times 3 @ 2$	Neither
	Conv $4 \times 4 @ 128$	BatchNorm
	ReLU + MaxPool	Neither
	Conv $4 \times 4 @ 256$	BatchNorm
	ReLU + MaxPool	Neither
	SoftMax	Neither

The proposed method is tested and evaluated on a computer with Inter Core I7-9700K at 3.6 GHz CPU, Gefore GTX 1080ti GPU with two 16 GB memories. The proposed method is implemented using the open-source PyTorch framework.



Figure 2. Optical images and corresponding SAR images of ten classes of objects in the MSTAR database. (From left to right: BMP2, BTR70, T72, 2S1, BRDM2, ZSU234, BTR60, D7, T62, and ZIL131.).

3.2. Recognition Performance under SOC

The recognition results of the proposed SFAS under standard operating condition (SOC) are shown in Table 3. From the table, facing 5-shot each target without pre-training, our method can achieve an 82.06% overall recognition ratio, and when the training number of each class in few labeled SAR samples is 20 and 10 respectively, the recognition rate just decreases from 94.18% to 89.28%. It indicates that the transductive generalization on unlabeled samples can improve the recognition performance when the labeled samples decrease. When the number of each class in few labeled SAR samples is 40, it gets above 95.5%, and eight classes of all targets are above 98.00%. It shows that the inductive bias constructed by the proposed SFAS is beneficial for the recognition of few labeled samples, though the two classes of the target are more sensitive to the decreased labeled samples. In addition, it is clear that, when the number of each class in few labeled SAR samples is larger than 80, the recognition rate can get above 98.5%. It demonstrates the effectiveness of the proposed SFAS in SAR ATR under few labeled SAR samples. When all the training samples are employed, the proposed method can achieve state-of-art performance in SAR ATR. -

[6] We have removed the bold in Table 3.

Table 3. Recognition accuracy (%) of SOC under different numbers of labeled images in each classes.

Class	Labeled Number in Each Class						
	5	10	20	40	80	100	All
BMP2	38.97	92.31	98.46	98.97	97.95	99.49	100.00
BTR70	93.80	98.18	97.45	100.00	99.49	98.47	100.00
T72	71.79	73.85	96.41	99.49	95.92	100.00	99.49
BTR60	100.00	98.47	96.41	94.36	98.46	98.97	97.44
2S1	98.91	86.50	93.80	81.39	98.54	98.91	97.81
BRDM2	67.52	93.07	100.00	99.64	100.00	98.91	100.00
D7	84.62	86.08	99.64	98.18	99.64	100.00	99.27
T62	93.37	83.67	80.24	89.01	98.53	99.64	100.00
ZIL131	86.86	93.43	91.84	98.54	97.45	97.81	100.00
ZSU234	77.74	84.67	90.15	99.64	98.54	100.00	100.00
Average	82.06	89.28	94.18	95.62	98.52	99.22	99.42

3.3. Recognition Performance under EOCs

In the practical application, there are more complex challenges in SAR ATR. For example, the training samples and testing samples are acquired under larger depression angle differences, which leads to obvious recognition failures. Therefore, in this subsection, the recognition performance under extended operating conditions (EOCs) such as the variances of the depression angle, target configuration, and version are evaluated for the robustness and effectiveness of the proposed SFAS.

Thanks to SAR images being sensitive to the depression angle, the experiments under a larger depression angle, EOC-D, are evaluated. The training and testing samples are listed in Table 4. The training samples are captured at 17°, and the testing samples are captured at 30°. The recognition performances under EOC-D are listed in Table 5. From Table 5, it is clear that our SFAS can achieve high performance under 100, 80 and 40 training samples for each class. Furthermore, when the training samples for each class are 20 and

10, respectively, the recognition performances of EOC-D are 94.61% and 90.18%. It has illustrated that our method can handle the few-shot effect under a large depression angle. -

[7] We have added a space between the "Test" and "(" in Table 4.

Table 4. Training and testing dataset under EOCs.

Train	Number	Test (EOC-D)	Number
2S1	299	2S1(b01)	288
BRDM2	298	BRDM2(E71)	287
T72	232	T72(A64)	288
ZSU234	299	ZSU234(d08)	288
Train	Number	Test (EOC-C)	Number
BMP2	233	T72(S7)	419
BRDM2	298	T72(A32)	572
BTR70	233	T72(A62)	573
T72	232	T72(A63)	573
		T72(A64)	573
Train	Number	Test (EOC-V)	Number
BMP2	233	T72(SN812)	426
		T72(A04)	573
BRDM2	298	T72(A05)	573
		T72(A07)	573
BTR70	233	T72(A10)	567
		BMP2(9566)	428
T72	232	BMP2(C21)	429

At the same time, the variances of target configuration and version, EOC-C and EOC-V, are evaluated for the effectiveness and practicability of our SFAS. The training and testing samples for EOC-C and EOC-V are listed in Table 4. The training samples are captured at 17°, and the testing samples for EOC-C and EOC-V are captured under 17° and 15°. The recognition performances for EOC-C and EOC-V are listed in Tables 6 and 7.

For the recognition performance of EOC-C, it is obvious that the SFAS can achieve high performance, even facing few samples for each class. When the numbers of training samples are larger than 20 for each class, the overall recognition performances are higher than 94%. In addition, the recognition ratio of 20 in each class is 94.23% and the recognition ratio of 10 in each class is 88.99%. When the number of training samples is decreasing from 100 to 20, the recognition of EOC-C is still effective. It indicated that the SFAS faced the few-shot effect and showed certain robustness under EOC-C.

Table 5. Recognition accuracy (%) of EOC-D under different numbers of labeled images in each class.

Class	EOC-D				
	Labeled Number in Each Class				
	100	80	40	20	10
BRDM2	99.65	99.30	99.65	99.65	100.00
2S1	98.96	98.61	98.61	99.65	99.31
T72-A64	92.71	92.36	87.85	83.33	73.26
ZSU234	98.61	97.22	98.61	95.83	88.19
Average	97.48	96.87	96.18	94.61	90.18

Table 6. Recognition accuracy (%) of EOC-C under different numbers of labeled images in each class.

EOC-C					
Class	Labeled Number in Each Class				
	100	80	40	20	10
T72-A32	97.73	97.73	96.85	96.15	95.99
T72-A62	98.95	97.73	97.03	94.94	92.32
T72-A63	97.73	95.81	93.54	93.54	92.15
T72-A64	93.19	93.19	92.50	91.97	86.56
T72sn-s7	99.05	97.14	96.90	94.51	93.32
Average	97.23	96.27	95.28	94.21	92.03

Table 7. Recognition accuracy (%) of EOC-V under different numbers of labeled images in each class.

EOC-V					
Class	Labeled Number in Each Class				
	100	80	40	20	10
BMP2sn-9566	90.65	91.36	89.49	63.08	58.18
BMP2sn-c21	90.91	90.68	90.21	84.38	56.41
T72sn-812	98.36	98.83	98.59	99.77	99.30
T72-A04	98.08	97.03	98.08	97.73	99.30
T72-A05	96.68	95.99	96.68	95.64	98.78
T72-A07	97.56	97.03	97.03	94.42	98.95
T72-A10	98.77	98.59	98.59	98.24	98.77
Average	96.16	95.88	95.85	94.23	88.99

From the recognition results of EOC-V, the recognition ratios under a different number of training samples for each class are higher than 90.000%. When the number of training samples is decreasing from 100 to 10, the recognition ratio under EOC-V is decreasing slowly and smoothly, from 97.23% to 92.03%. It has illustrated that the proposed SFAS has shown its effectiveness and robustness under EOC-V.

From the recognition performance of EOCs, the effectiveness and practicability of the proposed SFAS have been evaluated. For further validation, the segmentation results are shown as follows.

3.4. Segmentation Performance

The overall accuracy of the segmentation can achieve 99.10% for the segmentation of target and background. The computation equation of segmentation accuracy is quoted from [26]. The partial qualitative segmentation result of the proposed SFAS is shown in Figure 3. From the three rows, it is clear that the segmentation results are accurate compared with the ground truth. [A quantitative comparison regarding target accuracy, background accuracy, accuracy, and Intersection over Union \(IoU\) is listed in Table 8.](#) In conclusion, the proposed SFAS can employ the transductive generalization from auxiliary segmentation to improve the recognition of few labeled samples, and utilize the recognition features to back feed the segmentation.

[8] The color in Table 8 has been removed and we refer Table 8 here.

Table 8. Segmentation performance (%) of different methods.

Methods	Target Accuracy	Background Accuracy	Accuracy	IoU
Otsu	58.17%	88.35%	73.26%	52.10%
Canny	79.12%	90.13%	84.62%	72.01%
Ours	99.24%	98.97%	99.10%	98.23%

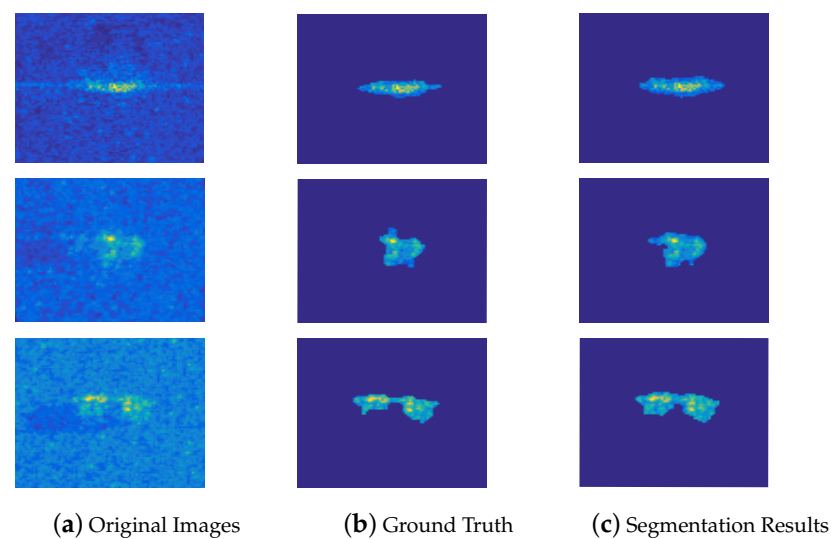


Figure 3. Three randomly selected samples to show the segmentation performance. Each row represents one sample including original image, ground truth, and segmentation result (from left to right).

3.5. Comparison and Ablation

Regarding the different numbers of labeled training images, we compare our methods with other SAR ATR methods, including five traditional methods (PAC+SVM, ADaboost, LC-KSVD, DGM, and Gauss) and few-shot learning methods. Among these few-shot learning methods, there are three data augmentation methods (GAN-CNN, MGAN-CNN, and ARGN), one metric-based methods (TMDC-CNNs), and four model-based methods (DNN1, DNN2, CNN, and Semisupervised). When the number of labeled training images is 20, 40, 80, and all samples from each target, it can be seen that our proposed SFAS achieves a higher recognition rate than other methods in Table 9. Even if the number of each target in the training dataset is only 20 samples, the recognition rate of our method is above 94%, while other methods are mostly below 86%. Therefore, the results can not only validate the effectiveness of our proposed SFAS in the case of employing all training images in the dataset but also in the case of few-shot learning. -

[9] We have removed the color and the bold in Table 9.

Table 9. Recognition accuracy (%) under different numbers of labeled images.

Method	Labeled Number					
	ALL	100	80	40	30	20
PCA+SVM [27]	94.32	-	92.48	87.95	-	76.43
ADaboost [9]	93.51	-	91.45	86.45	-	75.68
LC-KSVD [9]	95.13	-	93.23	87.39	-	78.83
DGM [9]	96.07	-	92.85	88.14	-	81.11
Gauss [28]	97.16	-	94.10	87.51	-	80.55
DNN1 [29]	95.54	-	93.04	86.98	-	77.86
DNN2 [30]	96.50	-	93.76	87.73	-	79.39
CNN [9]	97.03	-	93.88	88.35	-	81.80
GAN-CNN [9]	97.53	-	94.91	90.13	-	84.39
MGAN-CNN [9]	97.81	-	94.91	90.82	-	85.23
TMDC-CNNs [31]	-	99.09	-	-	86.93	-
ARGN [32]	98.00	-	95.98	-	87.20	-
Semisupervised [33]	-	-	98.65	97.11	-	92.62
The Proposed	99.42	-	98.52	95.62	-	94.18

For further automation and practicality, we utilized visual salience and morphological methods to automatically segment the target from the background, called auto-seg labels, and we replace the manual segmentation labels with the auto-seg labels to validate the effectiveness of our method. When the labeled samples are 40 and 20, the recognition ratios are 95.15% and 93.77%. It is clear that our method still achieves high performance under few-shot learning with rough auto-seg labels, which illustrated the effectiveness and practicability of our method.

The ablation experiments are also conducted shown in Table 10. When the labeled samples are 100, 80, 40, and 20, respectively, the recognition ratios without auxiliary segmentation loss are 98.93%, 95.09%, 84.62%, and 71.54% as shown in Table 10. The comparison illustrates that the segmentation loss is more effective facing few training samples.

Table 10. Ablation experiments of segmentation labels.

Sample Number	10	20	40	80	100
With segmentation loss	89.28	94.18	95.62	98.52	99.22
Without segmentation loss	62.57	71.54	84.62	95.09	98.93

3.6. Recognition Performance with Automatic Segmentation

In practice, samples with recognition labels may be impossible to obtain, and the segmentation label can be used to assist in recognizing small samples without recognition labels. Therefore, segmentation labels are helpful for recognition. If they are marked manually, it is really laborious, but some methods can automatically segment SAR images, which can also achieve recognition. We also conducted experiments to verify the above conclusions. We utilized visual salience and morphological methods to automatically segment the target from the background, called auto-seg labels. Then, we replace the manual segmentation labels with the auto-seg labels to validate the effectiveness of our method.

The recognition result of the proposed SFAS is shown in Table 11. The recognition ratio under a different number of training samples for each class is decreasing from 98.93% to 84.70%. When facing 100, 80 and 40 in each class, the recognition ratio achieved 98.93%, 95.67%, and 95.38%, respectively. It is clear that, with rough automatic segmentation, our SFAS still has the effectiveness and robustness of facing the few-shot effect. When the training samples for each class are 20 and 10, the overall recognition ratios with auto-segmentation are 93.19% and 84.70%. At the same time, the recognition ratios with manual segmentation are 94.18% and 89.28%. It showed that our SFAS still achieved good recognition performance and the precise segmentation can benefit the recognition. For the limited training samples, like 5-shot or 10-shot, our SFAS can employ precise segmentation from more effective segmentation methods for higher recognition ratios. -

[10] We have removed the bold in Table 11.

Table 11. Recognition accuracy (%) with automatic segmentation.

Class	Labeled Number in Each Class				
	10	20	40	80	100
BMP2	61.54	92.31	82.56	90.26	97.95
BTR70	66.06	84.67	95.62	88.69	98.91
T72	75.38	90.26	96.41	92.31	96.92
BTR60	71.43	88.78	89.29	97.45	99.49
2S1	95.62	90.88	94.16	93.07	99.27
BRDM2	94.53	97.08	92.70	99.27	98.91
D7	84.25	98.53	100.00	97.07	98.17
T62	97.45	97.96	99.49	99.49	100.00
ZIL131	93.43	95.99	100.00	98.18	99.27
ZSU234	97.81	94.53	99.64	100.00	100.00
Average	84.70	93.19	95.38	95.67	98.93

From the experiments with automatic segmentation, the practicability and effectiveness of our SFAS have been demonstrated. Even facing rough automatic segmentation, our SFAS still achieved high recognition performance and showed the robustness of the few-shot effect.

4. Conclusions

When the distributions of the few samples and complete samples have a large difference, the FSL of SAR ATR has failed to construct a helpful inductive bias. To tackle this challenge, we proposed a semi-supervised SAR ATR algorithm by employing a multi-level feature framework with auxiliary segmentation. By employing the supervised information of a few labeled samples and the transductive manifold of the unlabeled samples, the proposed novel SFAS exploits the transductive generalization to achieve better recognition performance of FSL in SAR ATR. Experimental results on the MSTAR dataset have validated the effectiveness and robustness of the proposed SFAS in few-shot recognition in SAR. The proposed SFAS not only can achieve the state of the art in recognition but also achieve superior performance in auxiliary segmentation.

Author Contributions: Conceptualization, C.W. and X.L.; methodology, C.W.; software, C.W.; validation, C.W., X.L., and Y.H.; formal analysis, Y.H. and J.P.; investigation, S.L., J.Y., and D.M.; resources, J.Y.; data curation, C.W. and X.L.; writing—original draft preparation, C.W. and X.L.; writing—review and editing, Y.H., J.P., and S.L.; visualization, C.W. and X.L.; supervision, J.Y. and D.M.; project administration, Y.H., J.P., J.Y., and D.M.; funding acquisition, J.Y. All authors have read and agreed to the published version of the manuscript.

Funding: This work was supported by the National Natural Science Foundation of China under Grants 61901091 and 61901090.

Data Availability Statement: This work does not report any data.

Conflicts of Interest: The authors declare no conflict of interest.

References

1. Geng, Z.; Yan, H.; Zhang, J.; Zhu, D. Deep-Learning for Radar: A Survey. *IEEE Access* **2021**, *9*, 141800–141818. <https://doi.org/10.1109/ACCESS.2021.3119561>.
2. Kechagias-Stamatis, O.; Aouf, N. Automatic Target Recognition on Synthetic Aperture Radar Imagery: A Survey. *IEEE Aerosp. Electron. Syst. Mag.* **2021**, *36*, 56–81. <https://doi.org/10.1109/MAES.2021.3049857>.
3. Oveis, A.H.; Guisti, E.; Ghio, S.; Martorella, M. A Survey on the Applications of Convolutional Neural Networks for Synthetic Aperture Radar: Recent Advances. *IEEE Aerosp. Electron. Syst. Mag.* **2021**, *37*, 18–42. <https://doi.org/10.1109/MAES.2021.3117369>.
4. Kechagias-Stamatis, O.; Aouf, N. Fusing Deep Learning and Sparse Coding for SAR ATR. *IEEE Trans. Aerosp. Electron. Syst.* **2019**, *55*, 785–797. <https://doi.org/10.1109/TAES.2018.2864809>.
5. Ding, B.; Wen, G. Target Reconstruction Based on 3D Scattering Center Model for Robust SAR ATR. *IEEE Trans. Geosci. Remote Sens.* **2018**, *56*, 3772–3785. <https://doi.org/10.1109/TGRS.2018.2810181>.
6. Sung, F.; Yang, Y.; Zhang, L.; Xiang, T.; Torr, P.H.; Hospedales, T.M. Learning to Compare: Relation Network for Few-Shot Learning. In Proceedings of the IEEE Conference on Computer Vision and Pattern Recognition (CVPR), Salt Lake City, UT, USA, 18–23 June 2018.
7. Wang, Y.; Yao, Q.; Kwok, J.T.; Ni, L.M. Generalizing from a Few Examples: A Survey on Few-Shot Learning. *ACM Comput. Surv.* **2020**, *53*. <https://doi.org/10.1145/3386252>.
8. Wang, L.; Bai, X.; Xue, R.; Zhou, F. Few-shot SAR automatic target recognition based on Conv-BiLSTM prototypical network. *Neurocomputing* **2021**, *443*, 235–246. <https://doi.org/10.1016/j.neucom.2021.03.037>.
9. Zheng, C.; Jiang, X.; Liu, X. Semi-supervised SAR ATR via multi-discriminator generative adversarial network. *IEEE Sens. J.* **2019**, *19*, 7525–7533.
10. Gao, F.; Yang, Y.; Wang, J.; Sun, J.; Yang, E.; Zhou, H. A deep convolutional generative adversarial networks (DCGANs)-based semi-supervised method for object recognition in synthetic aperture radar (SAR) images. *Remote Sens.* **2018**, *10*, 846.
11. Wang, L.; Bai, X.; Zhou, F. Few-Shot SAR ATR Based on Conv-BiLSTM Prototypical Networks. In Proceedings of the 2019 6th Asia-Pacific Conference on Synthetic Aperture Radar (APSAR), Xiamen, China, 26–29 November 2019; pp. 1–5.
12. Fu, K.; Zhang, T.; Zhang, Y.; Wang, Z.; Sun, X. Few-Shot SAR Target Classification via Metalearning. *IEEE Trans. Geosci. Remote Sens.* **2021**, *60*, 2000314.
13. Persello, C.; Bruzzone, L. Active and semisupervised learning for the classification of remote sensing images. *IEEE Trans. Geosci. Remote Sens.* **2014**, *52*, 6937–6956.

14. Li, D.; Zhang, Y. Adaptive Model-Based Classification of PolSAR Data. *IEEE Trans. Geosci. Remote Sens.* **2018**, *56*, 6940–6955. <https://doi.org/10.1109/TGRS.2018.2845944>.
15. Chen, Z.; Maji, S.; Learned-Miller, E. Shot in the dark: Few-shot learning with no base-class labels. In Proceedings of the IEEE/CVF Conference on Computer Vision and Pattern Recognition, Nashville, TN, USA, 20–25 June 2021; pp. 2668–2677.
16. Hou, Z.; Kung, S.Y. Few-Shot Learning Via Dependency Maximization and Instance Discriminant Analysis. In Proceedings of the 2021 IEEE 31st International Workshop on Machine Learning for Signal Processing (MLSP), Gold Coast, Australia, 25–28 October 2021; pp. 1–6. <https://doi.org/10.1109/MLSP52302.2021.9596284>.
17. Ye, H.J.; Sheng, X.R.; Zhan, D.C. Few-shot learning with adaptively initialized task optimizer: A practical meta-learning approach. *Mach. Learn.* **2020**, *109*, 643–664.
18. Chen, Y.; Liu, Z.; Xu, H.; Darrell, T.; Wang, X. Meta-Baseline: Exploring Simple Meta-Learning for Few-Shot Learning. In Proceedings of the IEEE/CVF International Conference on Computer Vision, Montreal, QC, Canada, 10–17 October 2021; pp. 9062–9071.
19. Zhang, P.; Li, M.; Wu, Y.; Li, H. Hierarchical conditional random fields model for semisupervised SAR image segmentation. *IEEE Trans. Geosci. Remote Sens.* **2015**, *53*, 4933–4951.
20. Jing, H.; Sun, X.; Wang, Z.; Chen, K.; Diao, W.; Fu, K. Fine building segmentation in high-resolution SAR images via selective pyramid dilated network. *IEEE J. Sel. Top. Appl. Earth Obs. Remote Sens.* **2021**, *14*, 6608–6623.
21. Ma, F.; Zhang, F.; Xiang, D.; Yin, Q.; Zhou, Y. Fast Task-Specific Region Merging for SAR Image Segmentation. *IEEE Trans. Geosci. Remote Sens.* **2022**, *60*, 1–16. <https://doi.org/10.1109/TGRS.2022.3141125>.
22. Ma, F.; Zhang, F.; Yin, Q.; Xiang, D.; Zhou, Y. Fast SAR Image Segmentation With Deep Task-Specific Superpixel Sampling and Soft Graph Convolution. *IEEE Trans. Geosci. Remote Sens.* **2022**, *60*, 1–16. <https://doi.org/10.1109/TGRS.2021.3108585>.
23. Jing, W.; Jin, T.; Xiang, D. Fast Superpixel-Based Clustering Algorithm for SAR Image Segmentation. *IEEE Geosci. Remote Sens. Lett.* **2022**, *19*, 1–5. <https://doi.org/10.1109/LGRS.2021.3124071>.
24. Wan, L.; Zhang, T.; Xiang, Y.; You, H. A Robust Fuzzy C-Means Algorithm Based on Bayesian Nonlocal Spatial Information for SAR Image Segmentation. *IEEE J. Sel. Top. Appl. Earth Obs. Remote Sens.* **2018**, *11*, 896–906. <https://doi.org/10.1109/JSTARS.2018.2792841>.
25. Hou, Q.; Zhou, D.; Feng, J. Coordinate attention for efficient mobile network design. In Proceedings of the IEEE/CVF Conference on Computer Vision and Pattern Recognition, Nashville, TN, USA, 20–25 June 2021; pp. 13713–13722.
26. Wang, C.; Pei, J.; Wang, Z.; Huang, Y.; Wu, J.; Yang, H.; Yang, J. When Deep Learning Meets Multi-Task Learning in SAR ATR: Simultaneous Target Recognition and Segmentation. *Remote Sens.* **2020**, *12*, 3863.
27. Srinivas, U.; Monga, V.; Raj, R.G. SAR automatic target recognition using discriminative graphical models. *IEEE Trans. Aerosp. Electron. Syst.* **2014**, *50*, 591–606.
28. O’Sullivan, J.A.; DeVore, M.D.; Kedia, V.; Miller, M.I. SAR ATR performance using a conditionally Gaussian model. *IEEE Trans. Aerosp. Electron. Syst.* **2001**, *37*, 91–108.
29. Morgan, D.A. Deep convolutional neural networks for ATR from SAR imagery. In *Algorithms for Synthetic Aperture Radar Imagery XXII*; International Society for Optics and Photonics: Bellingham, WA, USA, 2015; Volume 9475, p. 94750F.
30. Ding, J.; Chen, B.; Liu, H.; Huang, M. Convolutional neural network with data augmentation for SAR target recognition. *IEEE Geosci. Remote Sens. Lett.* **2016**, *13*, 364–368.
31. Guan, J.; Liu, J.; Feng, P.; Wang, W. Multiscale Deep Neural Network with Two-Stage Loss for SAR Target Recognition With Small Training Set. *IEEE Geosci. Remote Sens. Lett.* **2022**, *19*, 1–5. <https://doi.org/10.1109/LGRS.2021.3064578>.
32. Sun, Y.; Wang, Y.; Liu, H.; Wang, N.; Wang, J. SAR Target Recognition With Limited Training Data Based on Angular Rotation Generative Network. *IEEE Geosci. Remote Sens. Lett.* **2020**, *17*, 1928–1932. <https://doi.org/10.1109/LGRS.2019.2958379>.
33. Wang, C.; Shi, J.; Zhou, Y.; Yang, X.; Zhou, Z.; Wei, S.; Zhang, X. Semisupervised Learning-Based SAR ATR via Self-Consistent Augmentation. *IEEE Trans. Geosci. Remote Sens.* **2020**, *59*, 4862–4873.